Eur. Phys. J. D **8**, 93–99 (2000)

THE EUROPEAN PHYSICAL JOURNAL D

EDP Sciences

Temperature-dependent ionization potential of sodium clusters

J. Akola[1,a], A. Rytkönen[1], H. Häkkinen[2], and M. Manninen[1]

[1] Department of Physics, University of Jyväskylä, P.O. Box 35, 40351 Jyväskylä, Finland
[2] School of Physics, Georgia Institute of Technology, Atlanta, GA 30332-0430, USA

Received 16 April 1999 and Received in final form 6 July 1999

Abstract. The ionization potential of sodium clusters ($8 \leq N \leq 55$) at a finite temperature is studied using density functional theory and *ab initio* molecular dynamics. The threshold regions of the photoionization efficiency curves are deduced from the integrated IP distributions, which are obtained from the energy eigenvalues of the highest occupied Kohn-Sham states during molecular dynamics by applying a theoretically well-defined shift. The calculated ionization potentials are directly compared to the experimental values. The energetically best geometry of Na_{55} is found to be a slightly distorted icosahedron.

PACS. 36.40.Cg Electronic and magnetic properties of clusters – 36.40.Mr Spectroscopy and geometrical structure of clusters – 71.24.+q Electronic structure of clusters and nanoparticles

1 Introduction

Practically all experimental measurements of free metal clusters include charging of the clusters. This has to be done in order to be able to guide clusters using electromagnetic lenses and to detect them using mass spectrometers. For this purpose, the photoionization of clusters is the most commonly used method and is therefore also extensively studied. Especially the ionization potential (IP) of alkali metal clusters [1–6] has been a popular target, and the results are explainable using the simple jellium picture.

The photoionization process of clusters is a very complex phenomenon. In order to describe this process precisely and to reproduce the experimental cross-sections for a specific cluster, one has to take into account several complicating factors. These factors include the thermal motion of ions, the E1 transition matrix element between the initial and the final state of the ionized electron, the innercore ionization, the plasmons and the photodissociation of clusters. It is difficult to include all these factors into a single theory, and therefore it is not a surprise that there are not many studies on this subject. Some studies however have been made on the cross-sections of the alkali metal clusters by using both jellium [6–8] and *ab initio* models [9]. In the study by Koskinen and Manninen [6], the temperature-dependent cross-sections of Na and K clusters were also presented. In addition, the temperature-dependent ionization potentials for K and Ag clusters have been calculated by using an ellipsoidal jellium model [10].

Recently [11] we calculated the threshold regions of the theoretical photoionization efficiency (PIE) curves for Al_6 and Al_7 at different temperatures by using the eigenenergies of the highest occupied Kohn-Sham (KS) single-particle states during *ab initio* molecular dynamics. In this paper we apply the same method to sodium clusters and this time we take all the valence electrons into account in order to reproduce the experimental PIE curves measured by Kappes *et al.* [3]. As a by-product of the PIE curves we present here the theoretically determined temperature-dependent ionization potentials, which should be directly comparable with the experimental ones [3,4]. In addition to the photoionization problem, the ground state geometry of Na_{55} is also discussed.

We wish to point out that we are using a simple single-particle picture. Therefore we neglect the plasmon effects, which might be important even for small Na clusters [8] although the plasmon energy is clearly below the ionization threshold [12]. We also do not include any photodissociation effects into our study.

2 Method

The calculations are done by using the BO-LSD-MD (Born-Oppenheimer local-spin-density molecular dynamics) method [13]. In this method the valence electron density is calculated by solving the Kohn-Sham one-electron equations by using a suitable parameterization for the exchange-correlation part of the LSD approximation [14]. From the converged valence electron density the classical Hellmann-Feynman forces on ions are calculated which together with the Coulomb repulsion of the positive ion cores determine the total forces on ions, according to which structural optimization or classical molecular dynamics (MD) of ions are performed. We use plane waves combined

[a] e-mail: jeakola@snafu.phys.jyu.fi

with the fast Fourier transform techniques as the basis for the one-electron wave functions and norm-conserving, non-local, separable [15] pseudopotentials [16]. Since the method deals with a finite, non-periodic computational cell [13], the charging of the cluster does not introduce any additional computational complications.

The calculation of the ionization potentials for the whole set of isomers in an MD run is a very tedious process. In order to make our study more reasonable, we look for a connection between the highest occupied Kohn-Sham single-particle energy eigenvalue ϵ_{HOMO} and the IP. According to the Hartree-Fock theory and the Koopmans' theorem, there should be a simple relation $I = -\epsilon_{\mathrm{HOMO}}$, where I is the ionization potential. However, in the density functional theory one has to add an extra energy shift in order to get the equivalence [17] *i.e.*

$$I = -\epsilon_{\mathrm{HOMO}} + v_{xc}(\infty). \tag{1}$$

The extra energy shift $v_{xc}(\infty)$ is actually the asymptotic limit of the exchange-correlation potential and it has its origin in the continuous nature of the accurate density functional [18–20]. From our experience this term is practically a constant for a specific cluster size, regardless of the geometry of the cluster [11]. It is important to notice that the validity of the Koopmans' theorem is assumed also in equation (1). Therefore one should not use this formula for systems of only a few electrons.

The energy shift $v_{xc}(\infty)$ can also be defined in terms of IP and electron affinity (EA). Perdew and Levy [19] have shown that

$$\epsilon_{\mathrm{HOMO}} + \epsilon_{\mathrm{LUMO}} = -(I + A), \tag{2}$$

where A is the electron affinity and LUMO refers to the lowest unoccupied KS state. By using the fact $\epsilon_{\mathrm{HOMO}} \leq \epsilon_{\mathrm{LUMO}}$ together with equation (1) we see immediately that

$$v_{xc}(\infty) \leq \frac{I - A}{2}, \tag{3}$$

where the equality holds for the degenerate HOMO and LUMO levels and the upperbound $(I - A)/2$ of the energy shift is the chemical hardness. Usually the actual asymptotic limit of the exchange-correlation potential is well below the chemical hardness. Nevertheless, we have observed that for the icosahedral Al_{13} [21,22] $v_{xc}(\infty)$ is about 1.6 eV while the chemical hardness is 1.7 eV. The reason for this is the very small HOMO-LUMO gap of Al_{13}, which is a consequence of a highly degenerate electron structure (Al_{13}^- is electronically magic with 40 valence electrons).

In practice we perform molecular dynamics (time step of 5 fs) for a cluster at different temperatures and record the distribution of the absolute values of the highest occupied KS eigenenergies. By shifting this distribution by $v_{xc}(\infty)$, which we have calculated for a set of different isomers, we obtain a distribution for IP at a certain temperature. We can also include the inner KS states to this distribution, but we want to point out that we do not have as good theoretical justification for the use of the same energy shift $v_{xc}(\infty)$ for these states. However, we have noticed with aluminum clusters [21,22] by comparing the experimental photoelectron spectra [23] and the theoretical KS eigenenergies that the same $v_{xc}(\infty)$ could be used also for the inner states.

In this study our aim is to calculate the theoretical photoionization efficiency spectra. In order to do this, the IP distribution has to be integrated. As showed in our earlier paper [11] one should be able to reproduce the threshold region of the PIE curve quite well with this method. We want to extend our treatment also to the post threshold region. Therefore during the integration of the IP distribution we weight the KS single-particle states by an exponential step function

$$w_{\mathrm{i}}(E) = \mathrm{e}^{-\alpha(E-E_{\mathrm{i}})}\theta(E - E_{\mathrm{i}}), \tag{4}$$

where $\theta(E-E_{\mathrm{i}})$ is the Heaviside's step function. The value of α is determined from the experimental PIE curve [3], which usually shows an exponential decay. Similar decay has been seen also in the theoretical PIE curves for the jellium clusters [6].

Our model has one limiting approximation: the relative weight of each state is a constant. In order to get the real relative weights one has to calculate the transition matrix elements between the single-particle states and the continuum, which is not possible in the context of this study. These weights can be crucial, because for example s-states are known due to their limited E1 transition rules ($\Delta l = 1$) to have relatively smaller cross-sections than other states ($\Delta l = \pm 1$).

For the determination of the IP value from the PIE curve we employ two commonly used methods. The first one is the baseline intercept method, where one extrapolates the first linear rise of the PIE curve to the baseline. Although there is no theoretical justification for polyatomics, this method is usually considered to produce the adiabatic ionization potential (aIP). The second one is the error function fit [24], where one fits Gaussians to the derivative of the PIE curve. The first maximum is in terms of harmonic oscillator considered to correspond to the vertical ionization potential (vIP).

Finally, we want to emphasize that all the theoretical IP values in our distributions are vertical IP's. One should notice also that equation (1) deals with vIP. We believe, that for metal clusters, the ionization process is too fast to include relaxation, because in the classical picture the average time which the electron of Fermi velocity v_{F} spends inside the cluster of radius $R = r_{\mathrm{s}}N^{1/3}$ is very short. For example for Na_{55} this time is 1 fs, while the relaxation process itself takes 10^1-10^2 femtoseconds.

3 Results

The molecular dynamics data (except for Na_{55}) is obtained from the recent study of Rytkönen *et al.* [25], where the main emphasis was on the melting process of Na clusters. In this study, molecular dynamics were performed at a constantly increasing temperature (heating rate 5 K/ps).

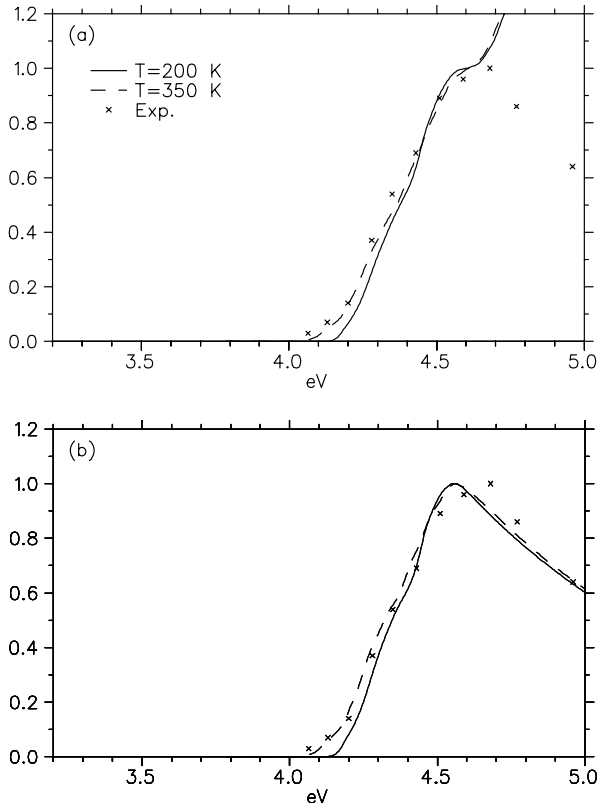

Fig. 1. The theoretically determined PIE curves for Na_8 at different temperatures compared to the experiments (crosses) [3]. (a) Heaviside's step function and (b) exponentially decaying step function are used in integration. The real theoretical curves are shifted by 0.25 eV in order to make the comparison to the experiments easier.

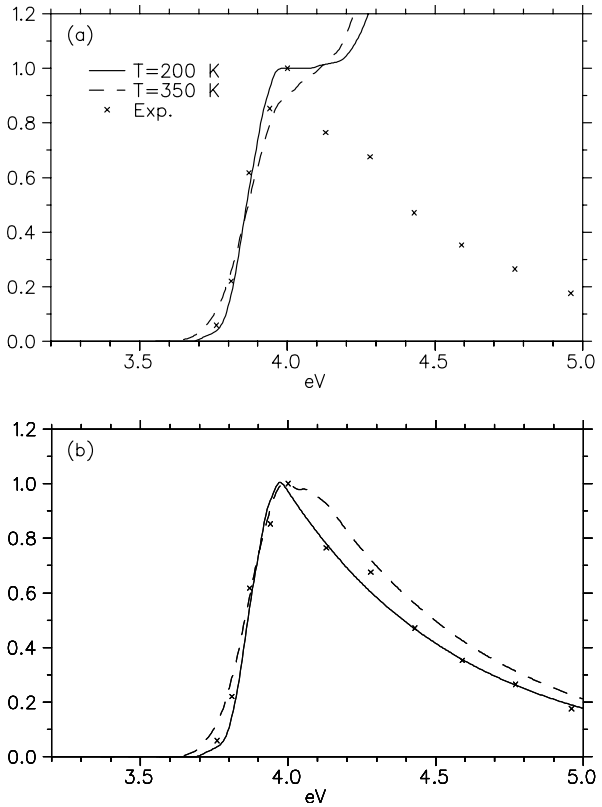

Fig. 2. Same as Figure 1 but for Na_{10} (the shift in the theoretical curves is 0.23 eV).

Therefore the data which we present here for a specific temperature is actually from a temperature range of 50 K, corresponding an MD run of 10 ps. The starting geometries of Na clusters and the simulations are thoroughly reported in the paper by Rytkönen *et al.* [25]. The overall temperature range in the simulations was around 150–400 K. All the calculations are done using the local density approximation (LDA). This means that also the energy shifts $v_{xc}(\infty)$ have been calculated using LDA instead of LSD, which causes naturally a small error.

In Figure 1 the integrated IP distributions of Na_8 are presented. For comparisonal purposes, these distributions are shifted with respect to the experiments. The experimental points represent mean values of the fluctuating signal [3]. The fluctuations are small close to the threshold and increase with increasing energy. Two different weights are used in integration: (a) a normal step function and (b) an exponentially decaying step function. The exponent parameter α in equation (4) is obtained from the experimental PIE curve [3] which is also presented in Figure 1. In both cases we have taken only the two highest occupied states into account, which means that we have given a zero weight for the underlying states. If also the third KS state (seen as a linear rise after the first maximum in Fig. 1a) is taken fully into account, then the energy of the maximum in the theoretical PIE curve is too far from the threshold value with respect to the experiments.

One can see by comparing Figures 1a and 1b, that the rising part of the PIE curve (where the experiment is more accurate) does not depend on the weighting procedure, which makes our exponential step function method reasonable. Comparison of the temperature shows that the slope of the theoretical PIE curve fits the experiments better at 350 K than at 200 K. Also the overall width of the PIE curve at 350 K is in good agreement with experiments while the PIE curve at 200 K is too narrow. Thus, we conclude that the experimental PIE curve of Na_8 corresponds well to our theoretical results at 350 K where the cluster should be essentially liquid.

The highest occupied KS state of Na_{10} is well-separated from the underlying states, which is consistent with the spherical jellium model (SJM). This is clearly seen in Figure 2a where the highest state at 200 K makes a clear step. When the temperature is increased to 350 K this step has significantly smeared out. By using the exponential weighting (Fig. 2b) for the highest occupied state alone one can see a considerable consistence with the experiments [3] at 200 K. One should also note that the experimental point around 4.2 eV, which does not fit into the theoretical curve, corresponds actually to the energy where the next underlying state starts to contribute. Also in Figure 2b the thermal broadening of the PIE curve is clearly seen. At 350 K the theoretical curve is definitely too wide and the slope of the rising part is too small.

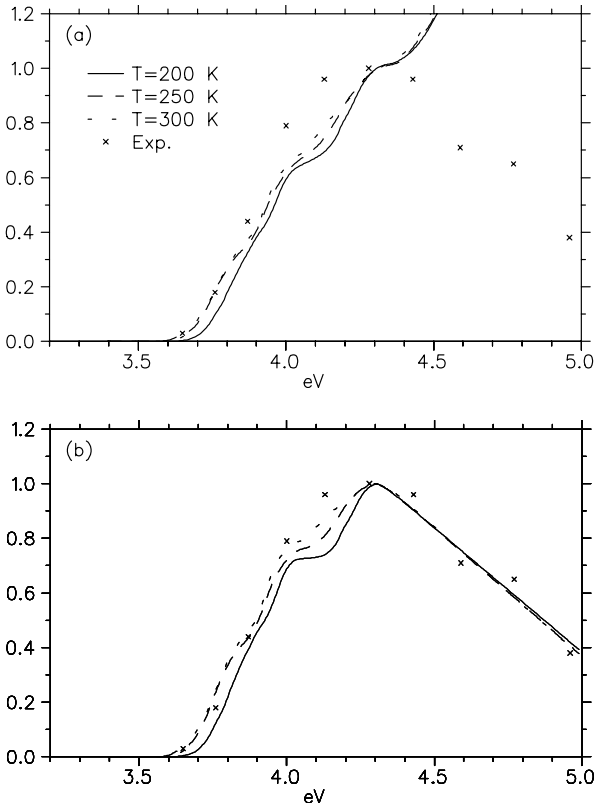

Fig. 3. Same as Figure 1 but for Na_{14} (the shift in the theoretical curves is 0.25 eV).

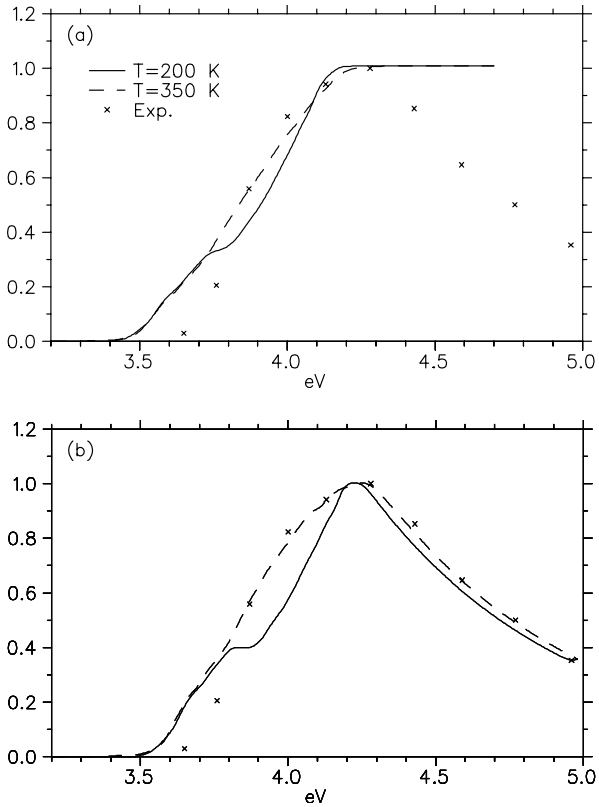

Fig. 4. Same as Figure 1 but for Na_{20} (the shift in the theoretical curves is 0.34 eV).

It is easy to conclude that a very good fit to the experiments is obtained at 200 K.

The three highest occupied states of Na_{14}, which correspond to 1*d*-states in the SJM, are in a bundle. Therefore the integrated and shifted IP distributions in Figure 3 are determined by giving all these states equal weights. For Na_{14} the decay mode of the experimental PIE curve is linear instead of exponential. This kind of a linear behaviour has been observed also for some potassium clusters [26], and in this case it is probably an effect of the first two underlying states (1*p*-states according to the SJM) which are not taken into account in the PIE curve determination. These states can actually be identified from the original PIE tail [3] by using our shifted KS energy eigenvalues.

Because the decay of the PIE curve of Na_{14} seems to be linear, we use a linear decay instead of the exponential one in Figure 3b. By comparing Figures 3a and 3b one can see that also here the rising part of the PIE curve does not depend considerably on the weight function although the bump before the maximum gets more pronounced. This bump corresponds to a region between the second and the third highest KS states and it starts to smear out when the temperature is increased. However, the temperature is not necessarily the explanation for the missing bump in the real PIE curve. The increasing single-particle cross-sections of the two highest states can also have a similar effect.

The deduction of the experimental temperature from Figure 3 is difficult, because the width of the theoretical PIE curves does not change much. Also the slopes of these curves are quite similar. According to Rytkönen *et al.* [25] Na_{14} (as well as Na_8 and Na_{10}) does not have any distinct melting transition region. This could be the explanation for the small temperature dependence of the theoretical PIE curves between 200–300 K.

In Figure 4 the integrated and shifted IP curve of Na_{20} is presented. Here all the 6 highest occupied KS states, which are in a bundle in accordance with the SJM, are taken into account in the PIE curve determination. The curves are fitted to the experimental values with respect to the maximum and the tail. There is no reasonable fit with respect to the threshold, and we believe that this is a consequence of a very low cross-section. It is well-known that the electronic structure of Na_{20} obeys the SJM very well. Therefore the highest occupied KS state (which is clearly seen in the theoretical spectra at 200 K) should have a 2*s*-type of a wavefunction, which should have a low cross-section.

The temperature effect on the theoretical PIE curves in Figure 4 is clearly visible as a broadening of the post threshold region. Nevertheless, the threshold region does not practically depend on the temperature at all. It means that the highest occupied KS state is insensitive to the temperature changes of the cluster. This also speaks on behalf of the 2*s*-type wavefunction, because we have seen similar behaviour for the 2*s*-state of Al_{13}^- icosahedron [22].

By comparing the post threshold regions of the PIE curves in Figure 4b, one can see that the theoretical curve

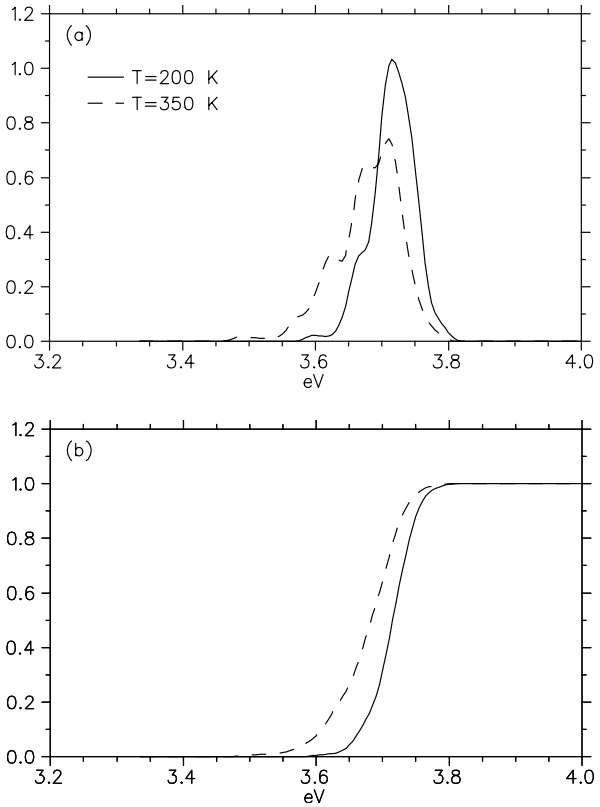

Fig. 5. (a) The IP distribution of Na_{40} at different temperatures and (b) the integrated threshold regions of the PIE curve. Only the highest occupied KS state is used here.

at 350 K is very close to the experimental one. We have indeed observed that by neglecting completely the highest state at 350 K, also the threshold region is very much similar to the experimental curve. Thus, we conclude that the experimental PIE curve corresponds quite well to our theoretical PIE curve at 350 K, where the cluster is liquid [25].

In Figure 5 we present the theoretical IP distributions of Na_{40} and the integrated threshold region of the theoretical PIE curve. One should note that only the highest occupied KS state is used here. The oscillations in Figure 5a have a statistical origin and are due to the limited time scale of our MD runs. According to the central limit theorem the IP distributions in Figure 5a should end up as Gaussians with large time scales. Usually this seems to be the case. However, there are clear exceptions such as Al_6 [11], where the IP distribution is limited to the IP of the ground state isomer.

The Na_{40} cluster melts around 300–350 K. This phase transition is also seen in the IP distributions in Figure 5a, where the increasing temperature displays the whole distribution by a certain value. The same effect is seen in the thresholds of the PIE curve in Figure 5b, where the whole threshold moves to the lower energies. Especially clear is the thermal tail effect in the beginning of the PIE curve, which increases strongly when the temperature gets higher.

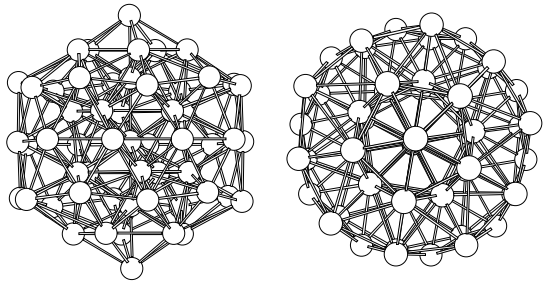

Fig. 6. The starting structure of Na_{55} for molecular dynamics.

As opposite to the smaller clusters, we do not have any melting run data for Na_{55}. Instead we made molecular dynamics for this cluster at a fixed temperature, which in this case was around 220 K. In Figure 6 the starting geometry of Na_{55} for the MD run is presented. This structure is optimized from the energetically best structure of Na_{55}^+ presented in the paper by Kümmel *et al.* [27]. The overall shape of this cluster is slightly oblate and it resembles very much an icosahedron because of its five fold symmetry. We also optimized the two other energetically favorable structures presented in reference [27], which were prolate and oblate. These isomers clearly had higher total energies in our calculations. The result that the nearly spherical cluster is the best structure is in contradiction with the predictions of the deformed jellium calculations [28–31], which predict that the electron density of 55 fermions wants to be prolate. Also in the melting simulations of Na_{55}^+ [25] prolate structures were observed for the melted Na_{55}^+. However, according to Kümmel *et al.* [27] the experimental photoabsorption spectrum and the calculated spectrum for the oblate and slightly oblate structure are in a good agreement, while there is no similarity for the prolate structure.

The energy eigenvalues of the highest occupied KS states during MD and the calculated density of states (DOS) for Na_{55} are presented in Figure 7. The eigenvalues and the distributions for the two lowest unoccupied states are drawn by using dashed lines. One directly sees that the HOMO and LUMO states are nearly degenerate. This is a consequence of SJM, which is applicable to this cluster because of the nearly spherical structure. One can also see the SJM effects in the initial KS energy eigenvalues, which occur in shells consistent to SJM.

During molecular dynamics there is a clear transition in the KS eigenvalues in Figure 7. The so called $1f$- and $1g$-states (according to SJM) split to two subshells. Because of this splitting, the collection of data for the DOS plot is started only after 4 ps. This effect also shows that our starting geometry is not yet the best possible structure, because the electron density clearly wants to deform. We see this also by optimizing two potential energy minimum structures from the end of our MD run. The optimized structures have the same total energy, and it is clearly lower than the total energy of our starting

Table 1. The determined theoretical IP values at 200 K compared to the experiments.

N	BO-LSD-MD: Error function fit	BO-LSD-MD: Baseline intercept	Ref. [4]: Baseline intercept	Ref. [3]: Baseline intercept	Ref. [3]: Watanabe	Ref. [3]: Pseudo-Watanabe
8	4.53	4.4		4.15	4.24	4.22
10	4.10	4.0		3.81	3.91	3.84
14	4.01	3.9 - 4.0	3.75	3.74	3.79	3.81
20	3.96	3.9	3.75	3.71	3.81	3.76
40	3.70	3.6 - 3.7	3.59			
55	3.59	3.5	3.41			

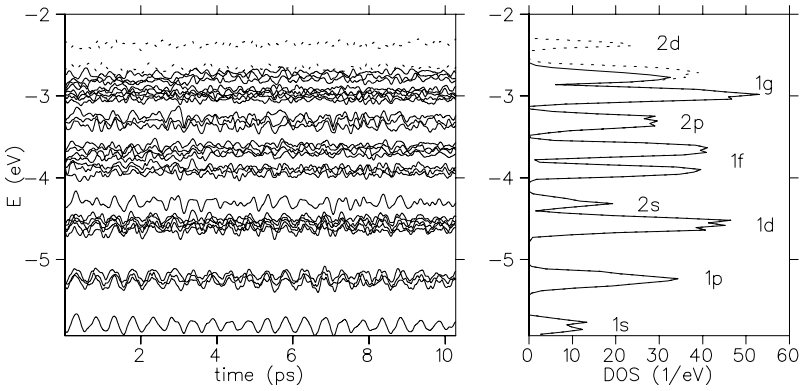

Fig. 7. The KS single-particle energy eigenvalues of Na_{55} during the molecular dynamics and the corresponding density of states. The DOS plot is started after 4 ps and the peaks are labeled by the SJM quantum numbers. Two lowest unoccupied states are drawn by using dashed lines.

geometry. The shape of these isomers does not differ much from a sphere: the first one is a slightly prolate and the second one is three axially slightly deformed. Icosahedral five fold symmetry patterns are seen for both of these clusters. In fact, this underlying icosahedral geometry does explain the splitting of the $1f$- ad $1g$-states (see Fig. 7a), because it is well-known that the icosahedral symmetry starts to perturb SJM states where $l \geq 3$. We believe that there are also slightly oblate geometries which have approximately the same total energies, because the shape of the cluster oscillates between oblate and prolate geometries during the MD run, while the features of the electron structure remain the same.

Finally, we present in Table 1 the determined ionization potentials at 200 K compared to the experiments [3,4]. We have chosen this temperature because in the experiments by Kappes *et al.* [3] the temperature is unknown and in the experiments by Persson *et al.* [4] it is below 100 K. Hence it is most convenient to use the data for the lowest temperature available. One can see that the theoretical IP values for small sodium clusters deviate 0.2–0.3 eV from the experimental ones. These errors are partly due to the use of the local density approximation, which always has a spin degeneracy even when the cluster has an odd number of electrons. For example for Na_{14} the use of LDA instead of LSD approximation causes an error of 0.06 eV. When the cluster size increases this error naturally gets smaller. One should note that the theoretical IP values for Na_{20} are determined from the highest occupied KS state, which in this case should be a $2s$-state, and therefore has a low cross-section. By using this argument as before we conclude that the actual error in the case of Na_{20} should be larger than 0.15 eV. For larger clusters (Na_{40} and Na_{55}) the IP values obtained by the baseline intercept method are closer to the experiments. We do not have any explanation for this behaviour besides the decreasing error due to the use of LDA.

4 Discussion and conclusion

In this paper we studied the temperature-dependent ionization process of small Na clusters by using a simple single-particle picture. Our aim was to reproduce and to explain the experimental PIE curves obtained for Na_8–Na_{20} [3]. By using the shifted KS energy eigenvalues and taking the exponential tail of the experimental PIE curve into account we were able to reproduce the experimental results quite well. The correspondence between the theory and experiments was especially good with Na_{10}, where the well-separated highest occupied KS state made our analysis easier.

According to our calculations, the experimental cluster temperatures for Na_8–Na_{20} seem to vary for different cluster sizes. The closed shell clusters Na_8 and Na_{20} have a considerably higher temperature ($T \approx 350$ K) than Na_{10} ($T \approx 200$ K). The temperature of Na_{14} is somewhere between these two temperatures. It is important to notice that the temperature range in our simulations is limited (200–350 K). Thus, it is possible that even better fits could be obtained for Na_8 and Na_{20} at higher temperatures. We believe that the reason for the different cluster temperatures is in the evaporation process. Because of the closed valence electron shells, the binding energy per atom

of Na_8 and Na_{20} is larger than for the other clusters in the same size range. Therefore these clusters tend to evaporate atoms less during the cooling process than others and their internal temperature should remain at a higher level.

Because there were not available any experimental PIE curves for Na_{40} and Na_{55}, we had to keep our PIE curve analysis in the threshold region, where only the highest occupied KS state was taken into consideration. For Na_{40} we observed a clear temperature effect, where the threshold of the PIE curve moved to the lower energies as the temperature was increased. Also the thermal tail effect was clearly visible for Na_{40}. For Na_{55} we cannot make any comparisons between different temperatures, because we performed MD only at 200 K. As for the smaller clusters, we could determine the theoretical ionization potentials for Na_{40} and Na_{55} at 200 K from the energy eigenvalues of the highest occupied KS states. The theoretical IP values are systematically higher than the experimental ones, but the error gets smaller when the cluster size increases.

According to our calculations the energetically best geometry of Na_{55} is a nearly spherical distorted icosahedron. This is in contradiction with the deformed jellium model for fermions [28–31]. At low temperatures the structural order of ions has a considerable effect on the total energy of the cluster. When the cluster is heated, this order disappears and the self-deformation of the electron density starts to dominate the total energy. In the case of Na_{55}^+, the electron density wants to be a prolate and the whole melted cluster deforms to a prolate shape. In fact, this kind of a temperature effect has been seen experimentally for large ($N \geq 923$) sodium clusters [32,33].

This work was supported by the Academy of Finland and the Väisälä Foundation. We want to thank Stephan Kümmel for communicating the results to us prior publication and Matti Koskinen for stimulating discussions.

References

1. W.A. de Heer, Rev. Mod. Phys. **65**, 611 (1993).
2. W.A. Saunders, Ph.D. thesis, University of California, 1986.
3. M. Kappes, M. Schär, U. Röthlisberger, C. Yeretzian, E. Schumacher, Chem. Phys. Lett. **143**, 251 (1988).
4. J. Persson, Ph.D. thesis, University of California, 1991; M.L. Homer, J.L. Persson, E.C. Honea, R. Whetten, Z. Phys. D **22**, 441 (1991).
5. C. Yannouleas, U. Landman, Phys. Rev. B **51**, 1902 (1995).
6. M. Koskinen, M. Manninen, Phys. Rev. B **54**, 14796 (1996).
7. O. Frank, J.M. Rost, Chem. Phys. Lett. **271**, 367 (1997).
8. M. Madjet, P.A. Hervieux, contribution to ISSPIC9.
9. B. Wästberg, A. Rosén, Z. Phys. D **18**, 267 (1991).
10. C. Yannouleas, U. Landman, Phys. Rev Lett. **78**, 1424 (1997)
11. J. Akola, H. Häkkinen, M. Manninen, Eur. Phys. J. D (in print).
12. T. Reiners, C. Ellert, M. Schmidt, H. Haberland, Phys. Rev. Lett. **74**, 1558 (1995).
13. R.N. Barnett, U. Landman, Phys. Rev. B **48**, 2081 (1993).
14. S.H. Vosko, L. Wilk, M. Nusair, Can. J. Phys. **58**, 1200 (1980); S.H. Vosko, L. Wilk, J. Phys. C **15**, 2139 (1982).
15. L. Kleinman, D.M. Bylander, Phys. Rev. Lett. **48**, 1425 (1982).
16. N. Troullier, J.L. Martins, Phys. Rev. B **43**, 1993 (1991).
17. D.J. Tozer, N.C. Handy, J. Chem. Phys. **108**, 2545 (1998); D.J. Tozer, N.C. Handy, J. Chem. Phys. **109**, 10180 (1998).
18. J.P. Perdew, R.G. Parr, M. Levy, J.L. Balduz, Phys. Rev. Lett. **49**, 1691 (1982).
19. J.P. Perdew, M. Levy, Phys. Rev. Lett. **51**, 1884 (1983).
20. J.P. Perdew, K. Burke, Int. J. Quantum. Chem. **57** (1996).
21. J. Akola, H. Häkkinen, M. Manninen, Phys. Rev. B **58**, 3601 (1998).
22. J. Akola, M. Manninen, H. Häkkinen, U. Landman, X. Li, L.-S. Wang, Phys. Rev. B **60**, 11297 (1999).
23. X. Li, H. Wu, X.-B. Wang, L.-S. Wang, Phys. Rev Lett. **81**, 1909 (1998).
24. H.G. Limberger, T.P. Martin, J. Chem. Phys. **90**, 2979 (1989).
25. A. Rytkönen, H. Häkkinen, M. Manninen, Phys. Rev. Lett. **80**, 3940 (1998); A. Rytkönen, H. Häkkinen, M. Manninen, Eur. Phys. J. D (in print).
26. C. Bréchignac, P. Cahuzac, Chem. Phys. Lett. **117** 365 (1985).
27. S. Kümmel, P.-G. Reinhard, M. Brack, contribution to ISSPIC9.
28. I. Hamamoto, B. Mottelson, H. Xie, X.Z. Zhang, Z. Phys. D **21**, 163 (1991).
29. S. Frauendorf, V.V. Pashkevich, Z. Phys. D **26**, S98 (1993).
30. S.M. Reimann, M. Brack, K. Hansen, Z. Phys. D **28**, 235 (1993).
31. S.M. Reimann, S. Frauendorf, M. Brack, Z. Phys. D **34**, 125 (1995).
32. T.P. Martin, S. Bjørnholm, J. Borggreen, C. Bréchignac, P. Cahuzac, K. Hansen, J. Pedersen, Chem. Phys. Lett. **186**, 53 (1991).
33. T.P. Martin, U. Näher, H. Schaber, U. Zimmermann, J. Chem. Phys. **100**, 2322 (1994).